Heterodyne Fourier domain optical coherence tomography for full range probing with high axial resolution

Adrian H. Bachmann [a), Rainer A. Leitgeb [a,b), Theo Lasser [a)

a) Laboratoire d'Optique Biomédicale, Ecole Polytechnique Fédérale de Lausanne, CH-1015 Lausanne, Switzerland
b) Center of Biomedical Engineering and Physics, Medical University of Vienna, Waehringerstrasse 13, A-1090 Vienna, Austria
rainer.leitgeb@epfl.ch

http://lob.epfl.ch

Abstract: One of the main drawbacks of Fourier domain optical coherence tomography (FDOCT) is the limited measurement depth range. Phase shifting techniques allow reconstructing the complex sample signal resulting in a doubled depth range. In current complex FDOCT realizations the phase shift is introduced via a reference path length modulation, which causes chromatic phase errors especially if broad bandwidth light sources are employed. With acousto-optic frequency shifters in the reference and sample arm, and the detector being locked to the resulting beating frequency, the signal is quadrature detected at high speed. The beating signal frequency is the same for all wavelengths allowing for achromatic complex reconstruction. With a Ti:Sapphire laser at $800nm$ and spectral width of $130nm$, a heterodyne complex FDOCT system is realized with $20kHz$ line rate and an axial resolution of $4\mu m$.

©2006 Optical Society of America

OCIS codes: (110.4500) Optical coherence tomography; (170.4500) Optical coherence tomography; (170.3880) Medical and biological imaging; (070.1060) Acousto-optical signal processing.

References and links

1. A. F. Fercher, C. K. Hitzenberger, G. Kamp, and S. Y El- Ziat,"Measurement of intraocular distances by backscattering spectral interferometry ," Opt. Commun. **117**, 43-48 (1995).
2. G. Häusler, M. W. Lindner," Coherence radar and spectral radar - new tools for dermatological diagnosis," J. Biomed. Opt. **7**, 21-31 (1998).
3. M. Wojtkowski, R. Leitgeb, A. Kowalczyk, T. Bajraszewski, A. F. Fercher," In vivo human retinal imaging by Fourier domain optical coherence tomography," J. Biomed. Opt. **7**, 457-463 (2002).
4. N. A. Nassif, B. Cense, B. H. Park, M. C. Pierce, S. H. Yun, B. E. Bouma, G. J. Tearney, T. C. Chen, J. F. de Boer," In vivo high resolution video rate spectral domain optical coherence tomography of the human retina and optic nerve," Opt. Express **12**, 367 (2004),
http://www.opticsexpress.org/abstract.cfm?URI=OPEX-12-3-367.
5. R. A. Leitgeb, C. K. Hitzenberger, A. F. Fercher "Performance of Fourier Domain vs. Time Domain optical coherence tomography," Opt. Express **11**, 889-894 (2003),
http://www.opticsexpress.org/abstract.cfm?URI=OPEX-11-8-889.
6. J. F. de Boer, B. Cense, B. H. Park, M. C. Pierce, G. J. Tearney, and B. E. Bouma,"Improved signal to noise ratio in spectral domain compared with time domain optical coherence tomography," Opt.. Lett. **28**, 2067-2069 (2003).
7. M. A. Choma, M. V. Sarunic, C. Yang, and J. A. Izatt,"Sensitivity advantage of swept source and Fourier domain optical coherence tomography," Opt. Express **11**, 2183-2189 (2003),
http://www.opticsexpress.org/abstract.cfm?URI=OPEX-11-18-2183.
8. E. Wolf," Three dimensional structure determination of semi transparent objects from holographic data," Opt. Commun. **1**,153-156 (1969).
9. A. F. Fercher, W. Drexler, C. K. Hitzenberger, T. Lasser,"Optical coherence tomography-principles and applications," Reports on progress in physics **66**, 239-303 (2003).

10. R. A. Leitgeb, W. Drexler, A. Unterhuber, B. Hermann, T. Bajraszewski, T. Le, A. Stingl, and A.F Fercher, "Ultrahigh resolution Fourier domain optical coherence tomography," Opt. Express **12**, 2156 (2004), http://www.opticsexpress.org/abstract.cfm?URI=OPEX-12-10-2156.

11. B. Cense, N. A. Nassif, T. C. Chen, M. C. Pierce, S. H. Yun, B. H. Park, B. E. Bouma, G. J. Tearney, and J. F. de Boer," Ultrahigh-resolution high speed retinal imaging using spectral-domain optical coherence tomography," Opt. Express **12**, 2435-2447 (2004), http://www.opticsexpress.org/abstract.cfm?URI=OPEX-12-11-2435.

12. M. Wojtkowski, T. Bajraszewski , I. Gorczynska, P. Targowski , A. Kowalczyk, W. Wasilewski, C. Radzewicz, "Ophthalmic imaging by spectral optical coherence tomography," Am J. Ophthalm. **138**, 412-419 (2004).

13. U. Schmidt-Erfurth, R. A. Leitgeb, S . Michels, B. Povaz¡ay, S. Sacu, B. Hermann, Ch. Ahlers, H. Sattmann, Ch. Scholda, A. F. Fercher, and W. Drexler, "Three-Dimensional Ultrahigh-Resolution Optical Coherence Tomography of Macular Diseases," Invest. Ophthalmol. Visual. Sci. **46**, 3396-3402 (2005).

14. M. Wojtkowski, V. Scrinivasan, T. H. Ko, J.G. Fujimoto, A. Kowalczyk, and J. S. Duker," Ultrahigh-resolution, high speed, Fourier domain optical coherence tomography and methods for dispersion compensation," Opt. Express **12**, 2404 (2004), http://www.opticsexpress.org/abstract.cfm?URI=OPEX-12-11-2404.

15. M. Wojtkowski, V. Srinivasan, J. G. Fujimoto, T. Ko, J. S. Schuman, A. Kowalczyk, J.S. Duker, "Three-dimensional Retinal Imaging with High-Speed Ultrahigh-Resolution Optical Coherence Tomography," Ophthalmology **112**,1734-1746 (2005).

16. A.F. Fercher, R. Leitgeb, C.K. Hitzenberger, H. Sattmann, M. Wojtkowski, "Complex spectral interferometry OCT," Proc. SPIE Vol. **3564**, 173 (1999).

17. M. Wojtkowski , R. Leitgeb, A. Kowalczyk, A. F. Fercher," Full range complex spectral optical coherence tomography technique in eye imaging," Opt. Lett. **27**, 1415-1417 (2002).

18. P. Targowski, M. Wojtkowski, A. Kowalczyk, T. Bajraszewski, M. Szkulmowski, I. Gorczynska, "Compelx spectral OCT in human eye imaging in vivo," Opt. Commun. **229**, 79-84 (2004).

19. J. Schmit and K. Creath, "Extended averaging technique for derivation of error-compensating algorithms in phase-shfiting interferometry," Appl. Opt. 34, 3610-3619 (1995).

20. P. Targowski, I. Gorczyńska, M. Szkulmowski, M.Wojtkowski, A. Kowalczyk, "Improved complex spectral domain OCT for in vivo eye imaging," Opt. Commun. **249**, 357-362 (2005).

21. Y. Yasuno, S. Makita, T. Endo, G. Aoki, H. Sumimura, M. Itoh, and T. Yatagai, "One-shot-phase-shifting Fourier domain optical coherence tomography by reference wavefront tilting," Opt. Express **12**, 6184-6191 (2004), http://www.opticsinfobase.org/abstract.cfm?URI=12-25-6184.

22. R. A. Leitgeb, C. K. Hitzenberger, and A. F. Fercher, "Phase shifting algorithm to achieve high speed long depth range probing by frequency domain optical coherence tomography," Opt. Lett. **28**, 2201-2003 (2003).

23. E. Götzinger, M. Pircher, R. Leitgeb, and C. Hitzenberger, "High speed full range complex spectral domain optical coherence tomography," Opt. Express **13**, 583-594 (2005), http://www.opticsinfobase.org/abstract.cfm?URI=oe-13-2-583.

24. M.A. Choma, C. Yang, J.A. Izatt, "Instantaneous quadrature low-coherence interferometry with 3x3 fiber-optic couplers," Opt. Lett. **28**, 2162 (2003).

25. S. H. Yun, G. J. Tearney, J. F. de Boer, and B. E. Bouma, "Motion artifacts in optical coherence tomography with frequency domain ranging," Opt. Express **12,** 2977- 2998 (2004), http://www.opticsexpress.org/abstract.cfm?URI=OPEX-12-13-2977.

1. Introduction

Fourier or spectral domain optical coherence tomography (FDOCT) is a biomedical imaging modality that gained increasing interest during the last years. The reason is its outstanding sensitivity that allows for high speed 2D and 3D imaging of weakly backscattering biological tissue in-vivo with high axial resolution [1-7].

The principle of FDOCT is based on the inverse scattering theorem that states that the inverse Fourier transform of the spectral interference pattern yields the axial sample structure [8,9]. Like in time domain OCT (TDOCT) the axial resolution increases with larger optical bandwidth of the employed light source (assuming that the spectrometer recording the spectral interferogram supports this bandwidth). However the achievable sensitivity of TDOCT decreases in the shot noise limit with increasing spectral width of the light source, i.e. with increasing axial resolution. On the other hand FDOCT sensitivity is independent of the spectral bandwidth [5]. Hence it was possible for the first time to perform clinical 3D imaging with ultrahigh resolution and in-vivo [10-15]. Nevertheless the achievable maximum depth range scales with the resolution of the spectrometer. Larger optical bandwidth results in reduced spectrometer resolution and thus in smaller depth range. In principle one could use a

detector with higher pixel number but this has severe implications on the optical design of the spectrometer to keep its diffraction limited performance. Also, the data volume to be dealt with increases with detector size and its handling becomes more challenging.

Another efficient way for increasing the depth range is achieved by generating the full complex signal [16]. The Fourier transform of the real valued spectrum yields redundant information for positive and negative frequencies corresponding to positive and negative path length differences between sample and reference. As a result one needs to adjust the reference arm delay so that it is slightly shorter than the relative distance of the first sample interface. In this case the axial structure does not mix with its mirrored representation in the adjoint Fourier half space. Hence only half of the Fourier space can be used for the sample structure. The reconstruction of the full complex signal resolves this ambiguity and the signal space is doubled [17]. This needs at least two phase-shifted copies of the cross correlation between sample and reference signal. The phase shift is commonly realized by changing the path length of the reference arm using for example a mirror mounted on a piezo actuator.
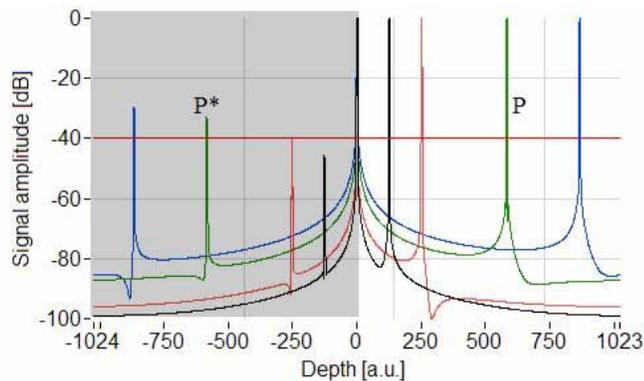

Fig. 1. Simulation of complex FDOCT signal reconstruction with chromatic phase shifting. Mirror terms in the left half (P*, grey shaded area) are not totally suppressed. The signals are normalized to the true signal peak amplitudes (P) in the right half space. The ratio between P* and P indicates the mirror term suppression. The simulation supposes a Gaussian spectral distribution with a spectral width (FWHM) of 20nm (black), 40nm (red), 90nm (green) and 130nm (blue) respectively. The central wavelengths are 800nm for all cases.

Shifting the reference optical delay Δz results in general in a chromatic phase error since the effective phase shift $\Delta \varphi$ is wavelength dependent, i.e. $\Delta \varphi(\lambda) = 4\pi \Delta z/\lambda$. First complex FDOCT systems used five phase-shifted signals and employed five-frame phase retrieval algorithms known from white light interferometry [16,17,18,19]. They have the advantage of being quasi achromatic and correct for the intrinsic phase error. Nevertheless they are only of limited use for in-vivo imaging since motion artifacts introduce stochastic phase errors that can only be handled by elaborate post processing algorithms [20]. Recently an alternative approach has been used where phase shifted spectra are recorded simultaneously on different lines of an area detector [21]. However the need for an area detector reduces the speed performance of the technique and the light efficiency is critical. Again five phase shifted spectral interference patterns have been selected to reconstruct the sample signal.

For small optical bandwidths, using reference phase shifting, it is sufficient to record only two spectra shifted by $\pi/2$ [22]. A fast and precise way of producing such phase shifted spectra has been demonstrated recently with an electro-optic modulator [23]. Nevertheless, if the chromatic phase error increases the mirror terms in the adjoint Fourier space will no longer be suppressed and the complex reconstruction fails. Fig. 1 shows a simulated complex FDOCT signal reconstruction based on the above two-frame algorithm for four different optical bandwidths (at 800nm central wavelength) keeping always the same ratio between spectral width of the spectrum and that of the spectrometer. The situation corresponds to the

interference between signals from two mirrors placed in the sample and reference arm. Fig. 2 shows the height ratio of the two adjoint peaks in both Fourier half spaces, *P* and *P**, depending on the optical bandwidth. Assuming a typical dynamic range in an OCT tomogram of 30 to 40*dB*, we observe that the mirror terms are sufficiently suppressed for standard resolution complex FDOCT. However, for high resolution systems with bandwidths above 40*nm* (for a Gaussian spectrum) the mirror terms become visible.
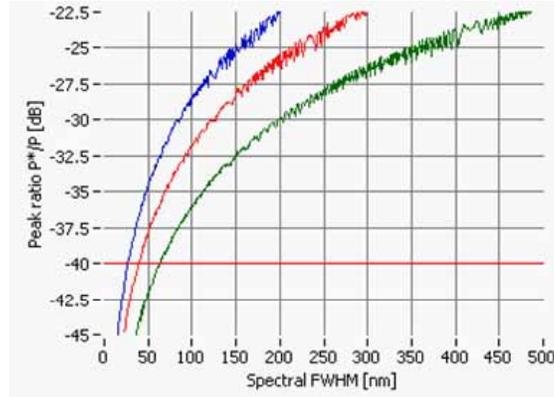

Fig. 2. The three plotted curves show the suppression ratio of P* (mirror term) with respect to P (signal peak) for three different central wavelengths of the light source depending on optical bandwidth (λ_0=550*nm* (blue), λ_0=800*nm* (red), λ_0=1300*nm* (green)). Above -40*dB* mirror terms become visible and the reconstruction algorithm fails. The "noisy" characteristics of the curves at larger bandwidths are due to leakage after discrete FFT.

A different complex two frame approach is based on the use of a 3x3 fiber coupler that allows simultaneous quadrature detection [24]. Despite its elegance there are some difficulties in particular with broad optical bandwidths concerning the fact that two individual but phase matched spectrometers are needed and that the actual splitting ratio of fiber couplers is wavelength dependent.

The current paper introduces a way for true achromatic complex FDOCT signal reconstruction by employing frequency shifting devices in order to create a beating signal with a wavelength-independent frequency on the spectrometer detector.

2. Heterodyne complex FDOCT

The most common way of introducing frequency shifts is by means of acousto-optic frequency shifters (AOFS). There, an ultrasonic wave is launched into an acoustic-wave-supporting material of usually high refractive index by means of a piezoelectric transducer. This acoustic wave alters the light frequency resulting in a constant and wavelength independent frequency shift of the original electromagnetic light field.

By employing two AOFS in the reference and sample path of an interferometer respectively, the frequency shifted light fields are $E_R(\omega_R',t,k) = \sqrt{I_R(k)}e^{j(k z_R-(\omega_0+\omega_R)t)}$ and $E_S(\omega_S',t,k) = \sum_i \sqrt{I_{S,i}(k)}e^{j(k z_i-(\omega_0+\omega_S)t)}$ with $\omega_{R,S}' = \omega_0 + \omega_{R,S}$ being the frequencies of the reference and the sample light fields after respective frequency shifting. The summation runs over all sample interfaces with $I_{S,i}(k)$ being the respective spectral intensities of the backscattered light fields and $I_R(k)$ the reference field intensity as functions of wavenumber *k*. $z_{i,R}$ denote the reference and sample interface positions. ω_0 is the frequency of the original light field and $\omega_{R,S}$ are the frequencies of the respective AOFS in the reference and sample path respectively. The interference field at the detector can then be written as

$$I(k) = I_R(k) + I_S(k) + \sum_{i,j;i\neq j} E_{S,i}(k) E_{S,j}^*(k) + \sum_i E_R(k) E_{S,i}^*(k) + c.c., \tag{1}$$

where $I_{R,S}(k)$ denote the reference and the total sample light intensities in the k-space with $E_R(k)$ and $E_{S,i}(k)$ as the reference and individual sample interface light fields and the asterix denoting their complex conjugates (*c.c.*). The first two terms on the rhs of Eq. (1) are DC terms, the second part together with its *c.c.* are autocorrelation terms due to interference of light fields from different sample interfaces. Only the last term and its *c.c.* contain the actual sample structure. By inserting the above described light field expressions into Eq. (1), one observes that only the cross-correlation term that represent the sample structure picks up a beating frequency $\Omega = |\omega_R' - \omega_S'| = |\omega_R - \omega_S|$. Denoting this term with its *c.c.* by I_{AC} we can write

$$I_{AC}(k,t) = 2\sum_i \sqrt{I_R(k)}\sqrt{I_{S,i}(k)}\cos(\Omega t - \Psi_i), \tag{2}$$

with Ψ_i containing all time-independent phase terms. Note that the frequency shifting gives rise to a wavelength independent phase term Ωt that governs the time dependence of the signal. If this signal is integrated over a certain time period, the modulation amplitude is reduced [25] and the recorded interference signal becomes

$$I_{AC,int}(k,t) = 2\sum_i \sqrt{I_R(k)}\sqrt{I_{S,i}(k)}\cos(\Omega t - \Psi_i)\,sinc\left(\frac{\tau\,\Omega}{2\pi}\right), \tag{3}$$

where τ is the integration or exposure time. This attenuation term is dependent on the ratio between integration time and beating period.

2.1 Complex FDOCT signal

The complex signal can finally be constructed if two spectral interference patterns with a $\pi/2$ phase difference are recorded. This is achieved by synchronizing the array detector with the beating frequency and by recording four spectra within one beating period. Hence successive spectra exhibit a phase difference of $\pi/2$. The complex signal becomes therefore [22]

$$\tilde{I}(k) = I(k,t_0) - jI\left(k,t_0 + \frac{\pi/2}{\Omega}\right), \tag{4}$$

at arbitrary time instant t_0. The important difference to previous complex FDOCT approaches is that according to Eq. (2) the phase difference between the two spectra is truly wavelength independent. Hence even large bandwidth sources can be employed without suffering from chromatic errors.

Since the signal phase changes continuously during detector exposure the signal intensity will be reduced according to Eq. (3). Nevertheless, the exposure time will always be smaller than a quarter of the beating period and therefore the attenuation cannot exceed -4*dB*. The above signal reconstruction resolves the complex ambiguity after performing the Fourier transform and leads therefore to a doubled depth range with respect to standard FDOCT [22]. Another important advantage regards the sensitivity of FDOCT. Due to the finite pixel size of the detector the modulation transfer function of the spectrometer decreases with increasing spectral modulation frequency, i.e., with increasing path length difference between sample and reference [5]. Hence the sensitivity is biggest close to the DC value. With a complex signal the structure can be placed across the DC line without being disturbed by its adjoint mirror terms.

It should be mentioned that with signal reconstruction based on Eq. (4) neither the DC nor autocorrelation terms will vanish after performing the Fourier transform. However,

autocorrelation terms are rather small in biological samples and the DC term can be strongly reduced by subtracting for example the separately recorded spectrum of the reference arm signal from each recorded spectrum before Fourier transform. An alternative way is to calculate a reference spectrum by averaging the recorded spectral interference patterns over a whole tomogram in post processing. In other approaches the complex conjugate of the signal in Eq. (4) is taken and the difference of the absolute values after the Fourier transform is calculated [22]. Such differential methods become critical especially if the structure strongly overlaps with its mirror image [23].

2.2 Differential complex reconstruction

Equation (4) is a two-frame method where two recorded interference patterns with a relative phase difference of $\pi/2$ constitute the complex signal. By subtracting two such complex signals with a relative time delay of half a beating period the parasitic DC and autocorrelation terms will efficiently be removed. This is due to the fact that these terms appear as static signals across the detector since their phase does not change with the beating frequency. As a result they will be eliminated already on the spectral level whereas the actual signal will be enhanced:

$$\tilde{I}_{2x2}(k) = \tilde{I}\left(k,t_0\right) - \tilde{I}\left(k,t_0+\frac{\pi}{\Omega}\right) =$$

$$= \left[I_{AC}\left(k,t_0\right) - I_{AC}\left(k,t_0+\frac{\pi}{\Omega}\right)\right] - j\left[I_{AC}\left(k,t_0+\frac{\pi/2}{\Omega}\right) - I_{AC}\left(k,t_0+\frac{3\pi/2}{\Omega}\right)\right] = \tag{5}$$

$$= 2\left(I_{AC}\left(k,t_0\right) - jI_{AC}\left(k,t_0+\frac{\pi/2}{\Omega}\right)\right).$$

After Fourier transform of Eq. (5) one is effectively left with the pure structure terms. Theoretically a signal enhancement of $3dB$ is obtained which counterbalances approximately the $-4dB$ signal loss mentioned in the previous section.

It is important to notice that the elimination of parasitic terms is insensitive to the exact phase difference of π between the two complex signals. Nevertheless the exact phase relation of $\pi/2$ is important for the respective two frames that constitute the complex signal.

3. Experimental

A Mach-Zehnder like interferometer setup as shown in Fig. 4 was built. The source is a mode-locked Ti:Sapphire laser (Femtolasers Inc.) with a central wavelength at $\lambda_0=800nm$ and a spectral full width at half maximum (FWHM) of $\Delta\lambda_{FWHM}=130nm$. The light is split via a 90:10 fiber coupler into the sample and reference arm respectively. The two pigtailed AOFS$_{1,2}$ (Brimrose Inc.) operate at 100 and $100.005MHz$ ($\omega_R = 2\pi \cdot 100.005MHz \pm 0.1Hz$ and $\omega_S = 2\pi \cdot 100MHz \pm 0.1Hz$). They generate a beating signal at the detector of the spectrometer at $5kHz$.
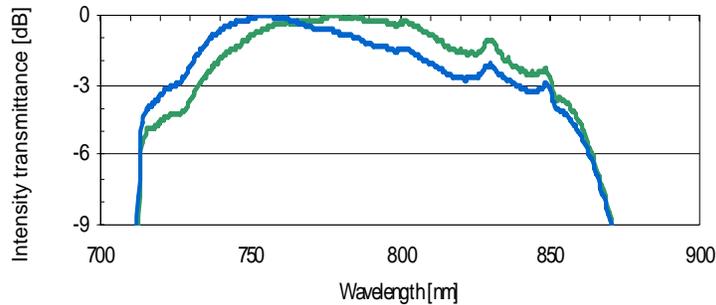

Fig. 3. Logarithmic spectral characteristics of the two pigtailed AOFS.

The spectral transmittance of the two AOFS is characterized by its -3dB width $\Delta\lambda_{-3dB} \approx 120nm$ (see Fig. 3). The translation stage (TS) in the reference arm is used for adjusting the relative delay to the sample. In order to exploit the full depth range the zero-delay is matched to the focal plane of the imaging optics. The dispersion mismatch between both arms is compensated by using BK7 wedges (DC). The scanning unit (Cambridge Technology) allows for a 2D scanning of the sample. For imaging an achromatic lens with a focal distance of 60mm is chosen resulting in a theoretical lateral resolution of 23.2μm and a depth of focus of 1.05mm. The transverse scanning speed across the sample is 30mm/s and the average illumination power 4.5mW. The array detector of the spectrometer is a 12bit line scan CCD with 2048 pixels (ATMEL AVIIVA), working at 20kHz and with an integration time of 30μs per acquisition. According to Eq. (3) the interference modulation amplitude is attenuated by -1.3dB. The detector trigger (Fig. 4(b)) is synchronized with the beating frequency (Fig. 4(a)) such that four equally delayed images within the full period of the beating signal are recorded (Fig. 4(c)). Since the phase changes continuously there is a constant $\pi/2$ phase shift between successive frames. Hence 'moving' two-frame reconstruction according to Eq. (4) is used as shown in Fig. 4(d). For the differential complex reconstruction four successive frames are used. However, the block of four frames constituting the next complex "A-scan" overlaps up to one frame with the previous block such that again a moving signal reconstruction is realized (Fig. 4(d)). As a result the actual number of complex "A-scans" per tomogram is equal to the number of recorded spectra minus three, which can be neglected. The spectrometer is equipped with a transmission diffraction grating of 1200lines/mm. The camera lens (CL) is a 135mm objective. The full spectral width covered by the spectrometer is $\Delta\lambda_{Spec}$=156nm. The actual FWHM of the spectrum at the detector is 90nm resulting in an axial resolution of 4μm in air. The measured sensitivity close to the zero delay is 111dB and decays by 15dB as one approaches the maximal depth position.
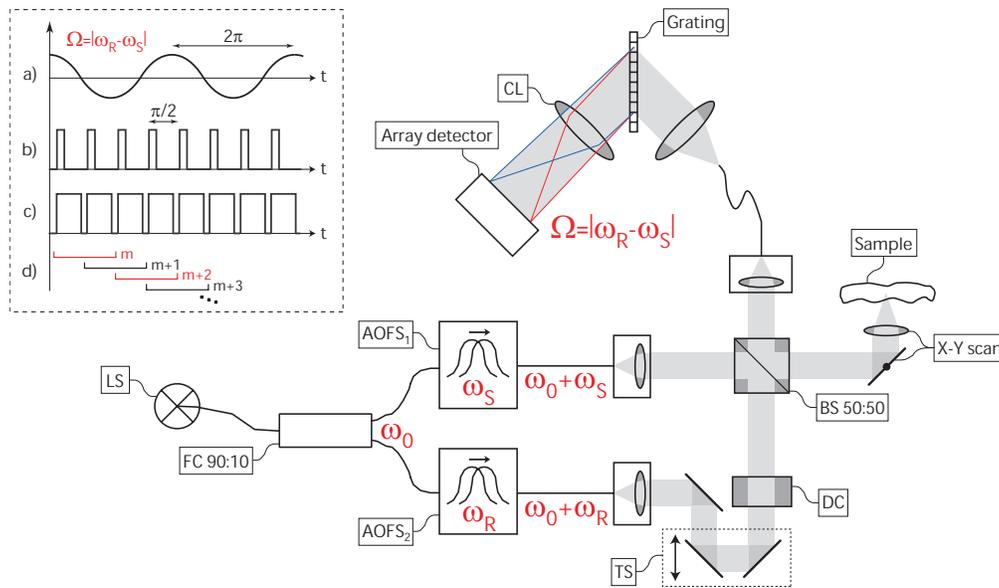

Fig. 4. Mach-Zehnder like interferometer comprising: Ti:Sapphire light source (LS), 90:10 fiber coupler (FC), AOFS shifting the light fields by $\omega_{R,S}$, translation stage (TS), dispersion compensation (DC), 50:50 beamsplitter (BS), galvo scanners (X-Y scan), camera lens (CL). Box in top left corner shows: (a) beating signal; (b) camera trigger; (c) camera exposure; (d) brackets indicate the frames used for complex two-frame reconstruction; different colors indicate frames used for differential complex technique.

4. Results and discussion

In order to test the heterodyne FDOCT setup in-vivo measurements on human skin were performed. Fig. 5 and Fig. 6 show tomograms with 2'000 "A-scans" and a lateral extension of 3*mm*. The acquisition time for a full tomogram was 100*ms*. The scanning was performed at continuous speed with a 15*x* over-sampling with respect to the theoretical lateral resolution.

Fig. 5 and Fig. 6 show the respective reconstructed sample structures of the nailfold region and of skin at the finger tip of an adult. The reference arm was adjusted such that the zero delay corresponded to a place within the structures. Fig. 5(a) and Fig. 6(a) show resulting tomograms using standard FDOCT without any DC correction, whereas for Fig. 5(b) and Fig. 6(b) a DC subtraction is applied in post processing (see §2.1). Standard FDOCT means that the recorded interference patterns that constitute a tomogram are first re-sampled to compensate for the spectrometer dispersion and to change from wavelength to wavenumber coordinate, and afterwards are Fourier transformed using FFT [3]. As a result of the complex ambiguity the structure is completely deteriorated by the overlapping mirror terms.
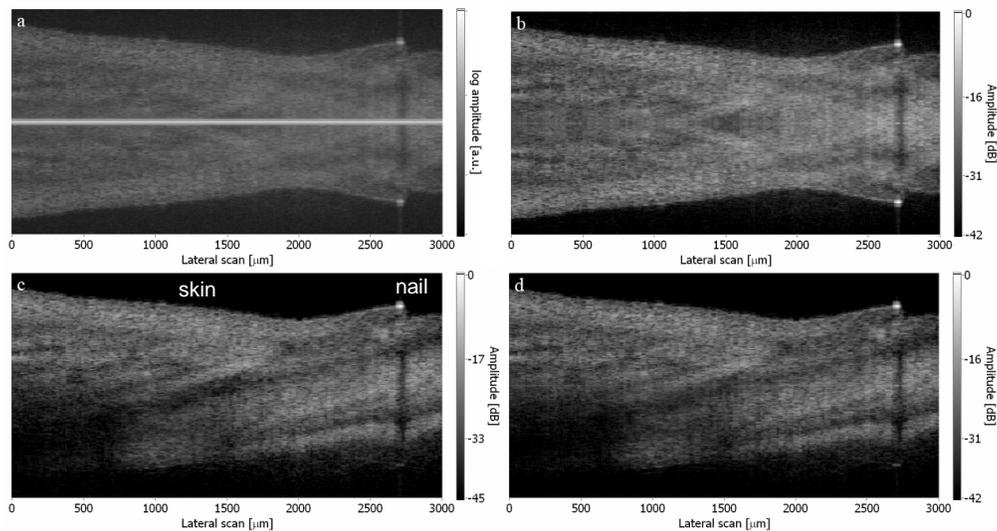

Fig. 5. (a) Tomogram of a fingernail fold region with standard FDOCT and no DC correction. The zero-delay is clearly visible due to the strong DC signal (bright line in the center). (b) As (a) but with calculated DC correction. (c) As (a) but reconstruction of complex signal according to differential complex method (see Eq.(5)) described in §2.2. (d) As (a) but reconstruction of complex signal according to Eq.(4) in §2.1 with a calculated DC correction. All tomograms are based on the same dataset. The tomogram depth shown is 1.75*mm* (in air).

Fig. 5(d) and Fig. 6(d) show the reconstruction of the tomogram using the two-frame method described by Eq. (4) in §2.1 with a DC correction. As one can see the structure is correctly reconstructed and the mirror terms are suppressed. Still, part of the DC term remains slightly visible but the influence on the image quality is negligible. Fig. 5(c) and Fig. 6(c) show the reconstruction of the tomogram using the differential complex algorithm described by Eq. (5) in §2.2. As for the two-frame reconstruction the structure is correctly displayed without its mirror terms but also the DC line is completely suppressed. The dynamic range of the tomograms lies between 40 and 45*dB*.
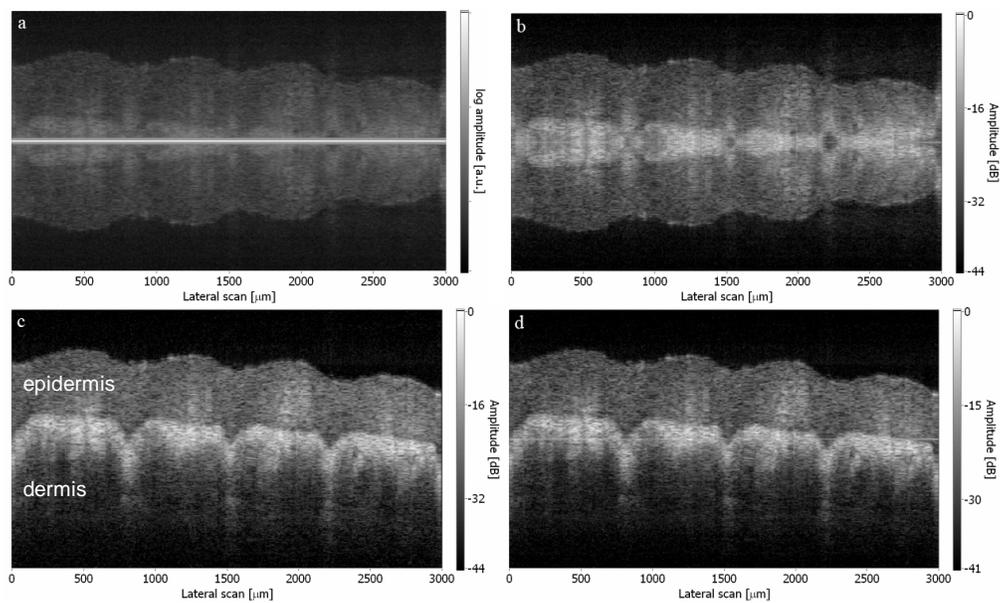
Fig. 6. (a)-(d) Same remarks as for Fig. 5. In-vivo object was a fingertip of an adult and the tomogram depth shown is 1.95*mm* (in air).

The fact that no reference spectrum must be recorded or calculated in post processing to suppress the DC component is an advantage of the differential complex reconstruction method. Moreover not only the DC part but also autocorrelation terms are suppressed and the dynamic range is improved by up to 3*dB* with respect to the two-frame complex reconstruction. Currently we are employing transverse over sampling in order to keep defined phase relation between consecutive spectra. As already mentioned in §2.2 the differential complex algorithm is relatively stable against phase errors. Nevertheless it is expected that with considerably lower transverse sampling the gain in dynamic range decreases and the suppression of the DC and autocorrelation terms will be less efficient.

In §3 it was pointed out that the sensitivity of FDOCT is highest close to the zero delay. By placing the object across the zero delay one has a clear advantage in sensitivity as compared to a situation where only half of the Fourier space is available. Especially for in-vivo applications structure movements are difficult to handle. For standard FDOCT enough distance to the zero delay needs to be kept in order to avoid overlapping with the mirror image. Thus, one sacrifices part of the high sensitivity of FDOCT and effective depth range. The tomograms in Fig. 5(c,d) and Fig. 6(c,d) demonstrate the sensitivity advantage for structures that cross the zero delay. Even for a central wavelength of 800*nm* it is possible to visualize dermal structures as shown in Fig. 6(c,d).

The main limitation of the current experimental realization is the fiberized AOFS with their -3*dB*-bandwidth of only 120*nm* as they reduce the axial resolving power of the system considerably.

5. Conclusion

In conclusion a high resolution FDOCT system has been realized that reconstructs the full complex signal content by quadrature detection of a stable beating frequency at 20'000 "A-scans" per second. The beating frequency is generated by two AOFS and is wavelength-independent; therefore no mirror terms interfere with the actual structure terms even if large bandwidth sources are employed. A novel differential complex reconstruction algorithm is proposed and experimentally verified that allows efficient elimination of DC and autocorrelation terms and shows a sensitivity advantage of approximately 3*dB* with respect to

a complex two-frame algorithm. The present achromatic, heterodyne system will exploit its full potential when combined with a true heterodyne detector that performs the signal demodulation for each pixel on-chip instead of an integrated bucket approach as in our case.

Acknowledgments